SCIENCE CHINA
Technological Sciences

•Article•

August 2024 Vol.67 No.8: 2405–2412
https://doi.org/10.1007/s11431-023-2555-y

Defect-mode and Fabry-Perot resonance induced multi-band nonreciprocal thermal radiation

CHEN ZiHe[1], YU ShiLv[1], YUAN Cheng[2], CUI XinYou[2] & HU Run[1*]

[1] *School of Energy and Power Engineering, Huazhong University of Science and Technology, Wuhan 430074, China;*
[2] *Wuhan Fiberhome Fuhua Electric Co., Ltd., Wuhan 430074, China*

Received June 2, 2023; accepted November 20, 2023; published online July 4, 2024

According to Kirchhoff's radiation law, the spectral-directional absorptivity (α) and spectral-directional emissivity (e) of an object are widely believed to be identical, which places a fundamental limit on photonic energy conversion and management. The introduction of Weyl semimetals and magneto-optical (MO) materials into photonic crystals makes it possible to violate Kirchhoff's law, but most existing work only report the unequal absorptivity and emissivity spectra in a single band, which cannot meet the requirements of most practical applications. Here, we introduce a defect layer into the structure composed of one-dimensional (1D) magnetophotonic crystal and a metal layer, which realizes dual-band nonreciprocal thermal radiation under a 3-T magnetic field with an incident angle of 60°. The realization of dual-band nonreciprocal radiation is mainly due to the Fabry-Perot (FP) resonance occurring in the defect layer and the excitation of Tamm plasmon, which is proved by calculating the magnetic field distribution. In addition, the effects of incident angle and structural parameters on nonreciprocity are also studied. What is more, the number of nonreciprocal bands could be further increased by tuning the defect layer thickness. When the defect layer thickness increases to 18.2 μm, tri-band nonreciprocal thermal radiation is realized due to the enhanced number of defect modes in the photonic band gap and the FP resonance occurring in the defect layer. Finally, the effect of defect location on nonreciprocity is also discussed. The present work provides a new way for the design of multi-band or even broad-band nonreciprocal thermal emitters.

Kirchhoff's law, multi-band nonreciprocal thermal radiation, magnetophotonic crystal, Tamm plasmon, defect layer, Fabry-Perot resonance

Citation: Chen Z H, Yu S L, Yuan C, et al. Defect-mode and Fabry-Perot resonance induced multi-band nonreciprocal thermal radiation. Sci China Tech Sci, 2024, 67: 2405–2412, https://doi.org/10.1007/s11431-023-2555-y

1 Introduction

Thermal radiation, one of the three forms of heat transfer, is widely used in energy harvest, transmission, conversion, and other fields [1–4]. In the last few decades, the design of high-efficiency thermal emitters has been provided with the development of nanophotonic technology, which is aimed at the efficient utilization of thermal radiation [5,6]. However, most current thermal emitters require that the emissivity e for a given angle and frequency is the same as the absorptivity α, i.e. $e(\theta,\lambda)=\alpha(\theta,\lambda)$ [7,8], which is the limitation of Kirchhoff's law. Under this law, when an object absorbs thermal radiation from the heat source, it must also emit energy to the heat source in the same direction, which will result in an inherent loss of energy [9–12]. Therefore, violating this detailed balance for higher energy recovery is necessary and meaningful.

Theoretically, Kirchhoff's law is not the requirement of the law of thermodynamics, but the result of the Lorentz reciprocity theorem [13]. In other words, the thermal emitters composed of nonreciprocal materials can break the restriction of Kirchhoff's law under certain conditions [14,15], to

*Corresponding author (email: hurun@hust.edu.cn)

realize the separate control of absorption and emission processes. For example, the utilization of magneto-optical (MO) materials can make the time-reversal symmetry break with an external excitation, so they are one of the ideal candidates for realizing nonreciprocal thermal radiation [16]. Despite promising prospects, the perfect nonreciprocal thermal emitters, i.e., $|\alpha - e| \to 1$, are still difficult to achieve. In 2014, Fan's group [14] designed a photonic crystal structure composed of an n-InAs grating structure and a metal layer. When the magnetic field B is 3 T, such structure demonstrates that the values of e and α are no longer equal, and the difference of $|\alpha - e|$ is close to 1 when the wavelength is 16 μm. Later on, in 2019, to reduce application conditions, Zhao et al. [17] proposed a nanophotonic design consisting of SiC grating and MO material InAs at the bottom. However, the grating structure is difficult to be processed and not easy to be prepared on a large scale, which makes it difficult to be applied in practice [18–20]. To simplify the fabrication process, Wu et al. [21] proposed a one-dimensional (1D) film structure composed of an MO layer and a spacer layer, which achieved the violation of Kirchhoff's law with a large magnetic field when the angle of incidence is 30°. More recently, type-I Weyl semimetals were found to be able to realize nonreciprocal radiation without an external excitation [15,22–24]. For example, Chen's group [24] proposed an optical nanostructure where a low-loss dielectric grating was added onto a semi-infinite magnetic Weyl semimetal, which can break Kirchhoff's law without any external stimulus. Nevertheless, all of these studies can only achieve single-band nonreciprocal thermal radiation, but most practical applications may require dual-band and even multi-band such as mid-infrared stealth, detectors, and filters [25,26]. Therefore, it is necessary to pay more attention to the design of dual-band and multi-band nonreciprocal thermal emitters.

Currently, the structures of nonreciprocal emitters mainly include 1D photonic crystal structure and grating structure. However, the grating structure is more complicated to fabricate due to the need for lithography technology. Therefore, more attention has been paid to the realization of multilayer nonreciprocal thermal emitters. The existing designs of dual-band and even multi-band nonreciprocal thermal emitters mainly include topological photonic crystal structures [27], epsilon-near-zero (ENZ) multilayer structures [28], and Thue-Morse multilayer structures [29]. More recently, we also proposed a design method for multi-band nonreciprocal multilayer thermal emitters [30]. However, due to the limitation of machining accuracy, the existence of defects in photonic crystals is a non-negligible problem in actual processing. The effect of defects on the properties of photonic crystals in reciprocal systems has been studied extensively [31–34], but the effect of defect layers on nonreciprocal thermal radiation is rarely studied. More recently, the integrated design of the Weyl semimetal and a photonic crystal with a defect layer can achieve the enhancement of the quality factor of nonreciprocal thermal radiation [22]. However, the influence of the defect layer on dual-band and even multi-band nonreciprocity is rarely reported.

In this work, we introduce the defect layer in 1D magnetophotonic crystals to achieve dual-band nonreciprocal thermal radiation. On this basis, we find that with the increase of defect layer thickness, a tri-band nonreciprocal emitter can be designed theoretically. The mechanism behind it is the excitation of Tamm plasmons and the Fabry-Perot (FP) resonance occurring in the defect layer, which can be proved by calculating the magnetic field distribution. Finally, the influences of incident angle, geometrical dimensions, and defect layer location on the nonreciprocal radiation are also investigated.

2 Theoretical model and method

The nonreciprocal emitter we proposed is shown in Figure 1, which is composed of a magnetophotonic crystal with a defect layer and the bottom metal layer Al. In this work, the magnetophotonic crystal is a 12-layer structure that consists of the MO material n-InAs and dielectric material SiO_2 and the unit layer thickness of the two materials is d and d_s, respectively. The defect layer is assumed as the MO material n-InAs and its thickness is d_d. In addition, a magnetic field B is along the y axis. Under the influence of an external magnetic field, the relative permittivity tensor of the doped InAs is nonsymmetric, and the specific expression is [35]

$$\varepsilon = \begin{bmatrix} \varepsilon_{xx} & 0 & \varepsilon_{xz} \\ 0 & \varepsilon_{yy} & 0 \\ \varepsilon_{zx} & 0 & \varepsilon_{zz} \end{bmatrix}, \tag{1}$$

where

$$\varepsilon_{xx} = \varepsilon_{zz} = \varepsilon_{\infty} - \frac{\omega_p^2(\omega + i\Gamma)}{\omega\left[(\omega + i\Gamma)^2 - \omega_c^2\right]}, \tag{2}$$

$$\varepsilon_{xz} = -\varepsilon_{zx} = i\frac{\omega_p^2\omega_c}{\omega\left[(\omega + i\Gamma)^2 - \omega_c^2\right]}, \tag{3}$$

$$\varepsilon_{yy} = \varepsilon_{\infty} - \frac{\omega_p^2}{\omega(\omega + i\Gamma)}. \tag{4}$$

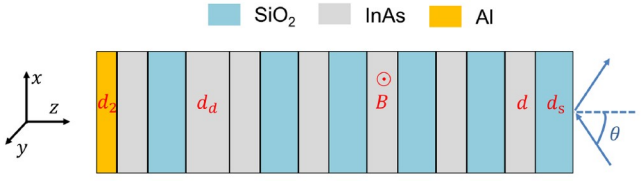

Figure 1 (Color online) Schematic of magnetophotonic crystal multilayer structure containing the defect layer.

The specific definitions and values of the above parameters are from the ref. [17]. The refractive index of the silicon dioxide is set at 1.45 and the permittivity of the metal Al is calculated by using the Drude model [17]:

$$\varepsilon_{\mathrm{Al}} = \varepsilon_{\infty} - \frac{\omega_{\mathrm{p}}^2}{\omega(\omega + i\Gamma)}, \tag{5}$$

where $\varepsilon_{\infty} = 1$, $\omega_{\mathrm{p}} = 2.24 \times 10^{16}$ rad/s and $\Gamma = 1.24 \times 10^{14}$ rad/s [17].

In addition, only transverse magnetic (TM) polarization wave in the *x*-*z* plane is considered and the angle of incidence is θ. The emissivity (e) and absorptivity (α) of this structure can be obtained by the calculations of the reflectivity and transmittance. Here, due to the high reflectivity of the metal Al, transmission processes are not considered. Therefore, the specific formulas of the α and e are [14]

$$\alpha(\theta,\lambda) = 1 - R(\theta,\lambda), \tag{6}$$

$$e(\theta,\lambda) = 1 - R(-\theta,\lambda). \tag{7}$$

The parameters $R(\theta,\lambda)$ and $R(-\theta,\lambda)$ are reflections of the angles of incidence θ and $-\theta$, respectively. The values of the corresponding reflection are calculated by using the transfer matrix method (TMM) and specific details can refer to refs. [16,35].

3 Results and discussion

In this work, the B is first set to 3 T, and it can be achievable in practice. On this basis, in order to obtain high emissivity, the material thickness is optimized, and the optimal results are as follows: d = 1.7 μm, d_{s} = 3.1 μm, d_{d} = 7.4 μm and d_2 (the thickness of the metal Al) = 0.2 μm. The angle of incidence θ is 60°. Here, in order to facilitate the distinction between different structures, $(AC)^6M$ represents the structure without a defect layer and $(AC)^5D(AC)M$ represents the structure containing a defect layer, in which the letters A, C, D and M respectively represent SiO_2, InAs, defect layer and metal layer.

Figure 2(a) shows the emissivity and absorptivity spectra of the structure $(AC)^6M$. It can be seen that the emissivity and absorptivity spectra are overlapped without an external excitation, i.e., $e(\theta,\lambda) = \alpha(\theta,\lambda)$. In this case, the structure is reciprocal and follows Kirchhoff's law. In addition, the sharp emission or absorption peak is achieved, which is mainly because Tamm plasmons are excited between the interface of the metal and photonic crystal. In contrast, when the applied magnetic field increases to 3 T, the emissivity and absorptivity spectra no longer coincide, i.e., $e(\theta,\lambda) \neq \alpha(\theta,\lambda)$. At the wavelengths of 15.760 and 16.035 μm, the difference between absorptivity and emissivity can approach 1, which shows the strong nonreciprocity. After introducing the defect into the structure, the emissivity and absorptivity spectra are calculated as shown in Figure 2(b). Similarly, when B = 0 T, there is no nonreciprocity. The difference is that another absorption (emission) peak occurs at the wavelength of 14.855 μm and the original peak is redshifted. With B = 3 T, both emission and absorption peaks show blueshift. The emissivity and absorptivity spectra also do not overlap with each other. The values of $|\alpha - e|$ at the wavelengths of 14.750 and 16.295 μm can reach 0.912 and 0.957, respectively, which exhibits the dual-band strong nonreciprocal thermal radiation and demonstrates that the existence of a defect layer can lead to the occurrence of dual-band nonreciprocal radiation. Then, the angular distributions of the absorptivity with B = 3 T at the wavelengths of 14.750 and 16.295 μm are calculated and the results are shown in Figure 2(c). It is obvious that the absorptivity is asymmetrical in spatial distribution, which is mainly attributed to the effect of the MO effect caused by InAs with an external excitation.

To better explain the mechanism behind it, the magnetic field distribution at the resonant wavelength is calculated. When there is no defect in the photonic crystal, the magnetic field distributions along the z direction at the wavelength of 15.760 μm with θ = 60° and θ = −60° are shown in Figure 3(a) and (b). It is obvious that the magnetic field

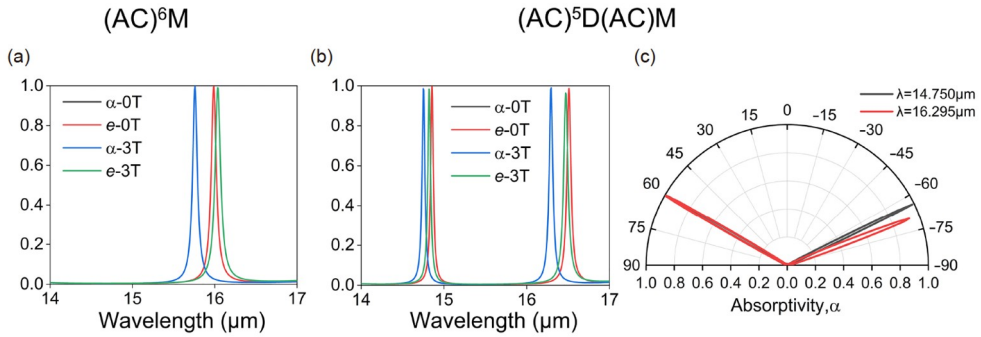

Figure 2 Absorptivity (α) and emissivity (e) spectra at θ = 60° with B = 0 T and B = 3 T. (a) The structure without the defect layer ($(AC)^6M$); (b) the structure with the defect layer ($(AC)^5D(AC)M$). (c) Angular distribution diagram of absorptivity at the resonant wavelengths with B = 3 T for the structure $(AC)^5D(AC)M$.

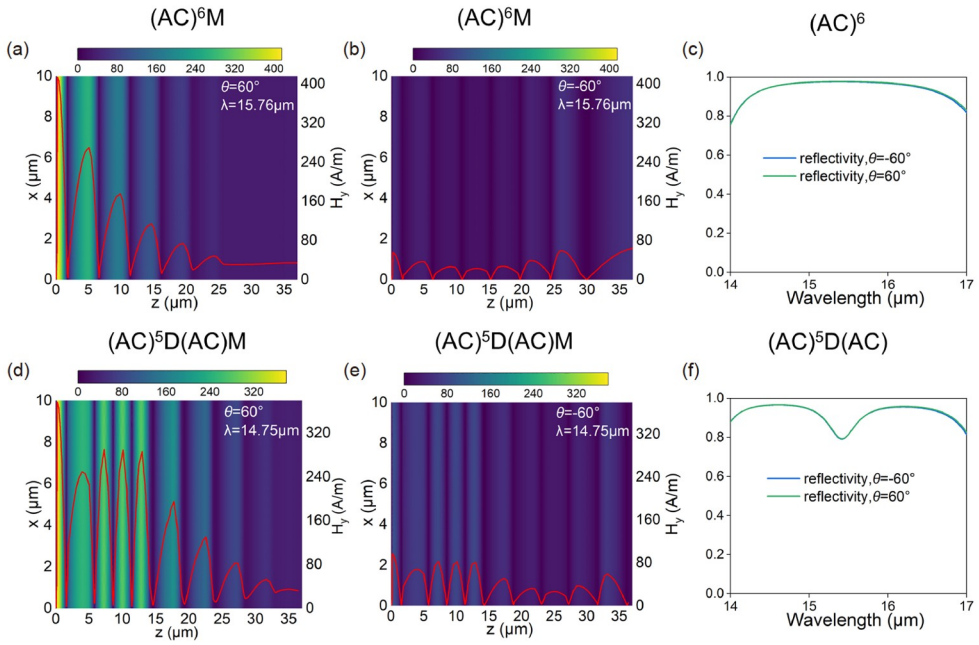

Figure 3 (Color online) Magnetic field distribution ($|H_y|$) of the structure $(AC)^6M$ along the z direction at the wavelength of 15.760 μm at (a) $\theta = 60°$ and (b) $\theta = -60°$ with $B = 3$ T. (c) The reflectivity spectra for the structure $(AC)^6$ at $\theta = 60°$ and $-60°$. Magnetic field distribution ($|H_y|$) of the structure $(AC)^5D(AC)M$ along the z direction at the wavelength of 14.750 μm at (d) $\theta = 60°$ and (e) $\theta = -60°$ with $B = 3$ T. (f) The reflectivity spectra for the structure $(AC)^5D(AC)$ at $\theta = 60°$ and $-60°$.

amplitude is greatly enhanced at the junction of metal and magnetophotonic crystal with $\theta = 60°$, which is mainly attributed to the excitation of Tamm plasmons. In addition, the magnetic field amplitude weakens when it is away from the metal, which further demonstrates the excitation of the Tamm plasmons at the junction of the metal and magnetophotonic crystal. Correspondingly, the enhancement of magnetic field amplitude can achieve a high absorption at the wavelength of 15.760 μm. When $\theta = -60°$, the barely enhanced magnetic field leads to a weak absorption of the structure. Therefore, the different magnetic field distributions in opposite directions lead to nonreciprocal radiation [35]. Figure 3(d) and (e) show the magnetic field distribution of the magnetophotonic crystal containing the defect layer at the wavelength of 14.750 μm. Compared with the magnetic field distribution of the structure without the defect layer, the magnetic field intensity does not decrease when it is away from the metal, but increases and presents the stationary wave mode along the z direction when z is between 5.8 and 14.6 μm, which is attributed to the FP resonance occurring in the defect layer. In addition, the excitation of Tamm plasmons can also be seen at the interface between metal and photonic crystals. What is more, to better understand the role of the defect layer in the photonic crystal, the reflection spectra of different structures are calculated respectively, as shown in Figure 3(c) and (f). It can be clearly seen that the presence of the defect splits the photonic band gap into two narrower band gaps, thus leading to dual-band nonreciprocal thermal radiation [29].

In order to deepen the understanding of the underlying physical mechanism, the effective impedance matching theory is adopted here for further explanation and specifically expressed as

$$Z = \sqrt{\frac{(1+S_{11})^2 - S_{21}^2}{(1-S_{11})^2 - S_{21}^2}}, \tag{8}$$

where S_{11} and S_{21} are the parameters related to scattering. In addition, because the bottom metal layer can block all transmissions, the parameter $|S_{21}|$ is equal to zero. Based on this, the effective impedances of the structures $(AC)^6M$ and $(AC)^5D(AC)M$ have been calculated respectively, as shown in Figure 4. First, when there is no defect layer, $Z = 0.969 - 0.101i$ with $\theta = 60°$ at the resonant wavelength of 15.760 μm, which is matched to the free space impedance $Z_0 = 1$ so that there is a strong absorption. By contrast, $Z = 0.016 - 1.298i$ with $\theta = -60°$ at the resonant wavelength of 15.760 μm, which is not matched so that there is a weak absorption. For the structure $(AC)^5D(AC)M$, the resonant wavelengths are 14.750 and 16.295 μm with $\theta = 60°$ and the corresponding effective impedances are $1.140-0.219i$ and $0.824+0.023i$. However, with $\theta = -60°$, the corresponding effective impedances are $0.022-0.376i$ and $0.091-3.126i$, which is not matched to Z_0. Therefore, by calculating the effective impedance, the nonreciprocity can be better understood.

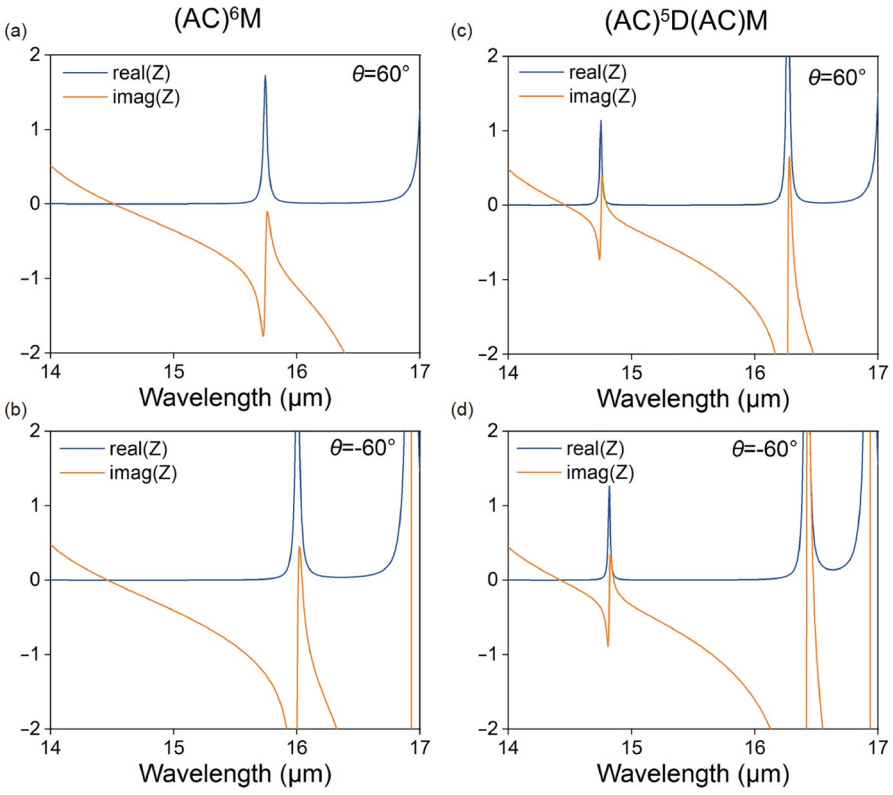

Figure 4 The effective impedance of the structure $(AC)^6M$ at (a) $\theta = 60°$ and (b) $\theta = -60°$ with $B = 3$ T. The effective impedance of the structure $(AC)^5D(AC)M$ at (c) $\theta = 60°$ and (d) $\theta = -60°$ with $B = 3$ T.

The nonreciprocal thermal radiation is closely related to the incident angle. Here, the absorptivity as functions of the wavelength and incident angle with $B = 0$ and 3 T is shown in Figure 5(a)–(d). When there is no defect in the magneto-photonic crystal, the absorptivity is symmetric with respect to $\theta \rightarrow -\theta$ without the external excitation, as shown in Figure 5(a). Compared with the bands in Figure 5(a), the band at $\theta < 0°$ shifts upward and the band at $\theta > 0°$ shifts downward when $B = 3$ T (Figure 5(b)). The asymmetry absorptivity with respect to the angle of incidence shows the violation of Kirchhoff's law. Compared with the absorptivity spectra of the structure $(AC)^6M$, there are two obvious absorption bands in Figure 5(c) and (d). Similarly, when the B is applied in the structure $(AC)^5D(AC)M$, the bands will shift and the dual-band nonreciprocal thermal radiation will be achieved.

Figure 5(e) and (f) give the value of $|\alpha - e|$ varying with the thickness of the material and wavelength at $\theta = 60°$ with $B = 3$ T. As shown in Figure 5(e), the thickness of InAs layer is changed from 0.1 to 5 μm, while keeping the thickness of SiO_2 unchanged. It can be seen that when d is in the range of 1.3–2.1 and 4–5 μm, dual-band nonreciprocal emitters can be obtained. Figure 5(f) shows the influence of d_s on the value of $|\alpha - e|$. The dual-band nonreciprocal radiation is realized when d_s is between 2 and 4 μm. Therefore, the dual-band nonreciprocal thermal emitter designed by this structure has a certain tolerance for size parameters.

Figure 6(a) discusses the influence of the defect layer thickness on the degree of nonreciprocity at $\theta = 60°$ with $B = 3$ T. The value of $|\alpha - e|$ as the function of the wavelength and defect layer thickness is calculated and the thickness of d_d is changed from 0.1 to 20 μm. The multiple pairs of separated bands can be seen in Figure 6(a), which represents the dual-band and even multi-band nonreciprocal radiation. Here, to show the effect of defect layer thickness on nonreciprocal thermal radiation more clearly, the difference between absorptivity and emissivity varying with the wavelength with $d_d = 18.2$ μm has been calculated which is part marked with red dots in Figure 6(a), as shown in Figure 6(b). It can be seen that the values of $|\alpha - e|$ at the wavelengths of 14.620, 15.615, and 16.495 μm can reach 0.862, 0.902, and 0.95, respectively. Such a phenomenon shows that multi-band nonreciprocal thermal radiation also can be achieved by adjusting the thickness of the defect layer, which provides a new way for designing multi-band nonreciprocal emitters. In addition, the reflectivity spectra for the structure $(AC)^5D(AC)$ at $\theta = 60°$ and $-60°$ when the thickness of the defect layer is 18.2 μm are calculated, as shown in Figure 6(c). Compared with the reflection spectra of the photonic crystal without the defect (Figure 3(c)), the complete photonic band gap is

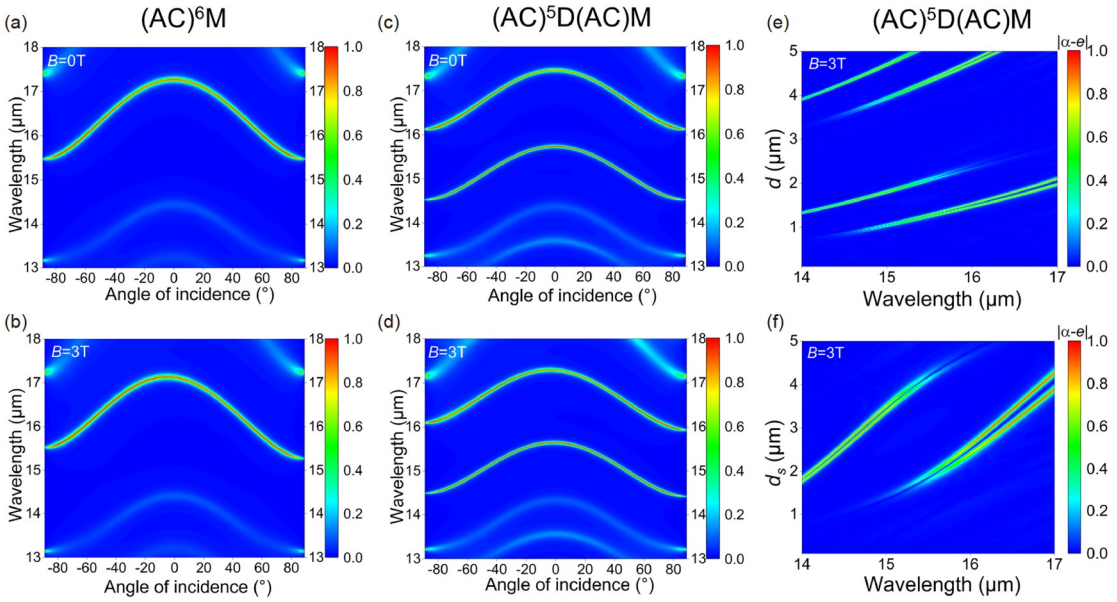

Figure 5 The absorptivity of the structure $(AC)^6M$ varies with the angle of incidence and wavelength: (a) B = 0 T; (b) B = 3 T. The absorptivity of the structure $(AC)^5D(AC)M$ varies with the angle of incidence and wavelength: (c) B = 0 T; (d) B = 3 T. (e) Difference between absorptivity and emissivity varies with the wavelength and the thickness of the InAs layer d. (f) Difference between absorptivity and emissivity varies with the wavelength and the thickness of the SiO_2 layer d_s.

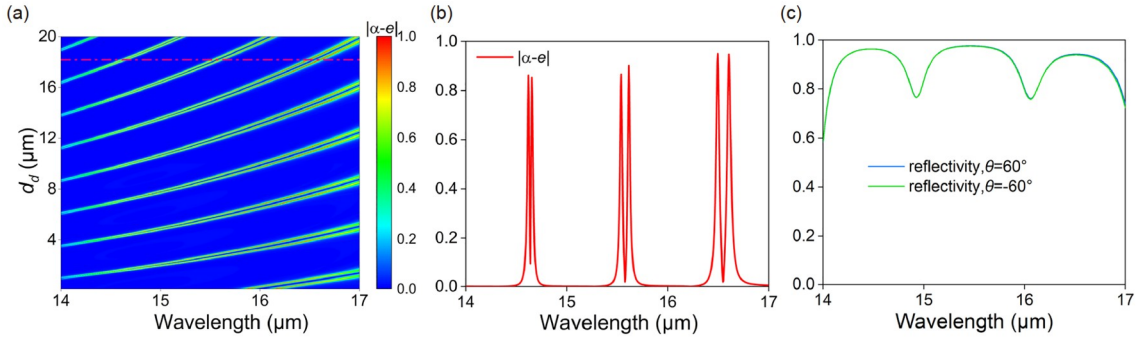

Figure 6 (a) Difference between absorptivity and emissivity varies with the wavelength and the thickness of the defect layer d_d. (b) The value of $|\alpha - e|$ when the thickness of defect layer is 18.2 μm. (c) The reflectivity spectra for the structure $(AC)^5D(AC)$ at $\theta = 60°$ and $-60°$ when the thickness of defect layer is 18.2 μm.

divided into three narrower photonic band gaps, corresponding to the tri-band nonreciprocal thermal radiation. Therefore, with the increase of defect layer thickness, more defect modes in the photonic band gap may lead to the realization of multi-band nonreciprocal thermal radiation [29].

To verify whether the influence of the location of the defect on the multi-band nonreciprocal thermal radiation is accidental, the nonreciprocities under different defect locations are discussed, as shown in Figure 7. For structures $(AC)D(AC)^5M$ and $(AC)^2D(AC)^4M$, as shown in Figure 7(a) and (b), there are two obvious nonreciprocal bands near 16 μm, which represent single-band nonreciprocal thermal radiation. In this case, even if there is a defect in the photonic crystal, it cannot form dual-band or even multi-band nonreciprocal thermal radiation well, mainly because the two ends of the defect layer are not highly reflective interfaces, which cannot form FP resonance. As the location of the defect layer gradually approaches the metal layer, as shown in Figure 7(c) and (d), it can be obviously seen that multiple pairs of separation bands appear with the increase of the thickness of the defect layer, representing dual-band and multi-band nonreciprocal thermal radiation. Therefore, by studying the effect of the location of the defect layer on the nonreciprocity, on the one hand, it shows that adding the defect layer to the photonic crystal can indeed achieve the regulation of multi-band nonreciprocal thermal radiation. On the other hand, it is also verified that whether FP resonance

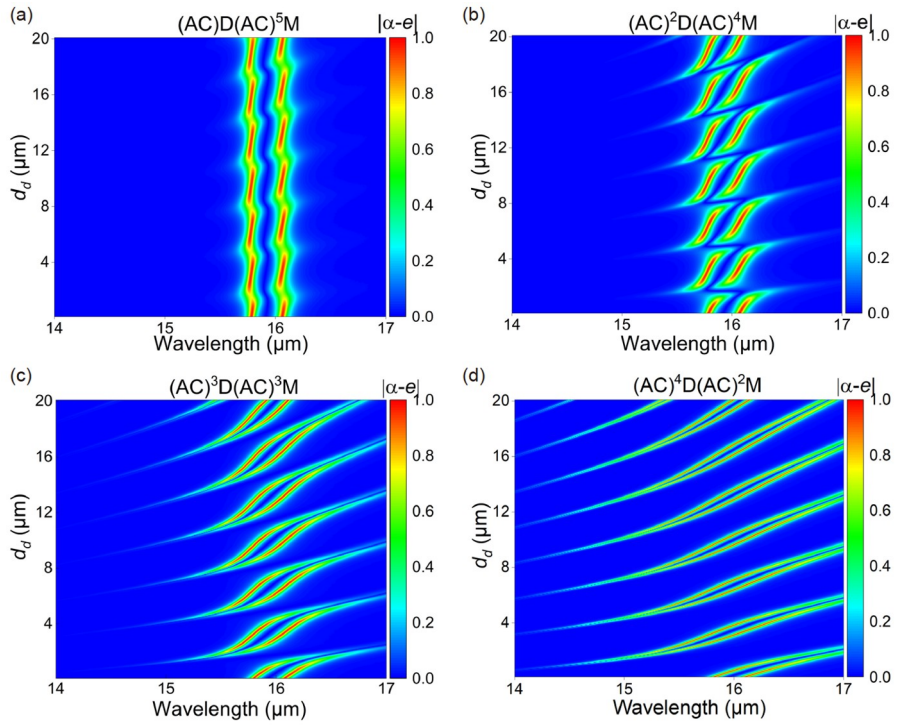

Figure 7 (Color online) Difference between absorptivity and emissivity varies with the wavelength and the thickness of the defect layer d_d for different structures. (a) (AC)D(AC)^{5}M; (b) (AC)^{2}D(AC)^{4}M; (c) (AC)^{3}D(AC)^{3}M; (d) (AC)^{4}D(AC)^{2}M.

can occur in the defect layer is an important prerequisite for the realization of multi-band nonreciprocal thermal radiation.

4 Conclusion

In summary, the emitter composed of magnetophotonic crystal with a defect layer and a metal layer can realize the dual-band nonreciprocal thermal radiation at $\theta = 60°$ with $B = 3$ T. The realization of dual-band nonreciprocal radiation is attributed to the FP resonance occurring in the defect layer and the excitation of Tamm plasmon, which can be demonstrated by calculating the magnetic field distribution. What is more, the defect layer thickness plays an important role in the number of nonreciprocal bands. When the thickness of the defect increases to 18.2 μm, tri-band nonreciprocal radiation is realized due to the enhanced number of defect modes in the photonic band gap. Finally, the location of the defect layer also has a great influence on the nonreciprocity, mainly because the location of the defect layer plays a crucial role in the formation of FP resonance. We believe that this work can provide new ways to design multi-band or even broadband nonreciprocal thermal emitters of practical interest.

This work was supported by the National Natural Science Foundation of China (Grant Nos. 52211540005, 52076087), the Open Project Program of Wuhan National Laboratory for Optoelectronics (Grant No. 2021WNLOKF004), Wuhan Knowledge Innovation Shuguang Program, and the Science and Technology Program of Hubei Province (Grant No. 2021BLB176).

1 Dalapati G K, Kushwaha A K, Sharma M, et al. Transparent heat regulating (THR) materials and coatings for energy saving window applications: Impact of materials design, micro-structural, and interface quality on the THR performance. Prog Mater Sci, 2018, 95: 42–131
2 Fan S. Thermal photonics and energy applications. Joule, 2017, 1: 264–273
3 Seyf H R, Henry A. Thermophotovoltaics: A potential pathway to high efficiency concentrated solar power. Energy Environ Sci, 2016, 9: 2654–2665
4 Liu P, Ren T T, Ge Y L, et al. Performance analyses of a novel finned parabolic trough receiver with inner tube for solar cascade heat collection. Sci China Tech Sci, 2023, 66: 1417–1434
5 Baranov D G, Xiao Y, Nechepurenko I A, et al. Nanophotonic engineering of far-field thermal emitters. Nat Mater, 2019, 18: 920–930
6 Li W, Fan S. Nanophotonic control of thermal radiation for energy applications. Opt Express, 2018, 26: 15995–16021
7 Kirchhoff G. Ueber das Verhältniss zwischen dem Emissionsvermögen und dem Absorptionsvermögen der Körper für Wärme und Licht. Annalen der Physik, 1860, 185: 275–301
8 Zhang Z M, Wu X, Fu C. Validity of Kirchhoff's law for semi-transparent films made of anisotropic materials. J Quantitative Spectr Radiative Transfer, 2020, 245: 106904
9 Rephaeli E, Fan S. Absorber and emitter for solar thermo-photovoltaic systems to achieve efficiency exceeding the Shockley-Queisser limit. Opt Express, 2009, 17: 15145–15159
10 Snyder W C, Wan Z, Li X. Thermodynamic constraints on reflectance reciprocity and Kirchhoff's law. Appl Opt, 1998, 37: 3464–3470
11 Buddhiraju S, Santhanam P, Fan S. Thermodynamic limits of energy harvesting from outgoing thermal radiation. Proc Natl Acad Sci USA, 2018, 115: E3609–E3615

12 Zang H W, Li H L, Liang T F, et al. Goldilocks focal zone in femtosecond laser ignition of lean fuels. Sci China Tech Sci, 2022, 65: 1537–1544
13 Han S E. Theory of thermal emission from periodic structures. Phys Rev B, 2009, 80: 155108
14 Zhu L, Fan S. Near-complete violation of detailed balance in thermal radiation. Phys Rev B, 2014, 90: 220301
15 Zhao B, Guo C, Garcia C A C, et al. Axion-field-enabled nonreciprocal thermal radiation in Weyl semimetals. Nano Lett, 2020, 20: 1923–1927
16 Liu M Q, Zhao C Y. Near-infrared nonreciprocal thermal emitters induced by asymmetric embedded eigenstates. Int J Heat Mass Transfer, 2022, 186: 122435
17 Zhao B, Shi Y, Wang J, et al. Near-complete violation of Kirchhoff's law of thermal radiation with a 0.3 T magnetic field. Opt Lett, 2019, 44: 4203–4206
18 Wu F, Wu J, Guo Z, et al. Giant enhancement of the Goos-Hänchen shift assisted by quasibound states in the continuum. Phys Rev Appl, 2019, 12: 014028
19 Wu J, Wu F, Zhao T, et al. Dual-band nonreciprocal thermal radiation by coupling optical Tamm states in magnetophotonic multilayers. Int J Thermal Sci, 2022, 175: 107457
20 Wu J, Wu F, Wu X. Strong dual-band nonreciprocal radiation based on a four-part periodic metal grating. Optical Mater, 2021, 120: 111476
21 Wu X, Liu R, Yu H, et al. Strong nonreciprocal radiation in magnetophotonic crystals. J Quantitative Spectr Radiative Transfer, 2021, 272: 107794
22 Wu J, Li H, Fu C, et al. High quality factor nonreciprocal thermal radiation in a Weyl semimetal film via the strong coupling between Tamm plasmon and defect mode. Int J Thermal Sci, 2023, 184: 107902
23 Luo M, Xu Y, Xiao Y, et al. Strong nonreciprocal thermal radiation by optical Tamm states in Weyl semimetallic photonic multilayers. Int J Thermal Sci, 2023, 183: 107851
24 Tsurimaki Y, Qian X, Pajovic S, et al. Large nonreciprocal absorption and emission of radiation in type-I Weyl semimetals with time reversal symmetry breaking. Phys Rev B, 2020, 101: 165426
25 Ning R, Jiao Z, Bao J. Tunable multi-band absorption in metasurface of graphene ribbons based on composite structure. Eur Phys J Appl Phys, 2017, 79: 10201
26 Liu Y J, Xie X, Xie L, et al. Dual-band absorption characteristics of one-dimensional photonic crystal with graphene-based defect. Optik, 2016, 127: 3945–3948
27 Wu J, Qing Y M. Strong nonreciprocal radiation with topological photonic crystal heterostructure. Appl Phys Lett, 2022, 121: 112201
28 Zhang Z, Zhu L. Broadband nonreciprocal thermal emission. Phys Rev Appl, 2023, 19: 014013
29 Wu J, Qing Y M. A multi-band nonreciprocal thermal emitter involving a Weyl semimetal with a Thue–Morse multilayer. Phys Chem Chem Phys, 2023, 25: 11477–11483
30 Chen Z, Yu S, Hu B, et al. Multi-band and wide-angle nonreciprocal thermal radiation. Int J Heat Mass Transfer, 2023, 209: 124149
31 Fang Y T, Zheng J. Optical isolator based on nonreciprocal coupling of two Tamm plasmon polaritons. Radiat Effects Defects Solids, 2014, 169: 1010–1018
32 Qi L, Yang Z, Fu T. Defect modes in one-dimensional magnetized plasma photonic crystals with a dielectric defect layer. Phys Plasmas, 2012, 19: 012509
33 Wu C J, Wang Z H. Properties of defect modes in one-dimensional photonic crystals. PIER, 2010, 103: 169–184
34 King T C, Wu C J. Properties of defect modes in one-dimensional symmetric defective photonic crystals. Physica E-Low-dimensional Syst NanoStruct, 2015, 69: 39–46
35 Wu J, Wang Z, Wu B, et al. The giant enhancement of nonreciprocal radiation in Thue-Morse aperiodic structures. Optics Laser Tech, 2022, 152: 108138